Importance of atmospheric aerosol pollutants on the degradation of Al 2 O 3 encapsulated Al-doped zinc oxide window layers in solar cells

Shan-ting Zhang, Alina Maltseva, Gunilla Herting, Jean-françois Guillemoles, Nathanaelle Schneider, Inger Odnevall, Polina Volovitch

Received: 7 September 2021 | Revised: 8 November 2021 | Accepted: 1 December 2021

DOI: 10.1002/pip.3527

RESEARCH ARTICLE

PROGRESS IN PHOTOVOLTAICS WILEY

Importance of atmospheric aerosol pollutants on the degradation of Al_2O_3 encapsulated Al-doped zinc oxide window layers in solar cells

Shan-Ting Zhang[1] | Alina Maltseva[2] | Gunilla Herting[3] | Jean-François Guillemoles[1] | Nathanaelle Schneider[1] | Inger Odnevall[3] | Polina Volovitch[2]

[1]CNRS, Ecole Polytechnique, IPParis, Chimie ParisTech, PSL University, IPVF SAS, UMR 9006, Institut Photovoltaïque d'Ile-de-France (IPVF), Palaiseau, France

[2]Chimie ParisTech, PSL University, CNRS, Institut de Recherche de Chimie Paris (IRCP), Paris, France

[3]KTH Royal Institute of Technology, Department of Chemistry, Division of Surface and Corrosion Science, Stockholm, Sweden

Correspondence
Polina Volovitch, Chimie ParisTech, PSL University, CNRS, Institut de Recherche de Chimie Paris (IRCP), 11 rue Pierre et Marie Curie, Paris 75005, France.
Email: polina.volovitch@chimieparistech.psl.eu

Inger Odnevall, KTH Royal Institute of Technology, Department of Chemistry, Division of Surface and Corrosion Science, Drottning Kristinas väg 51, Stockholm SE 100 44, Sweden.
Email: ingero@kth.se

Shan-Ting Zhang, CNRS, Ecole Polytechnique, IPParis, Chimie ParisTech, PSL University, IPVF SAS, UMR 9006, Institut Photovoltaïque d'Ile-de-France (IPVF), 18 boulevard Thomas Gobert, Palaiseau 91120, France.
Email: shanting.zhang@ipvf.fr; zhangst@sari.ac.cn

Abstract

Atmospheric aerosol pollutants are considered for the first time for the durability evaluation of non-metallic photovoltaic materials on the example of pristine and Al_2O_3-encapsulated Al-doped zinc oxide (AZO) window layers. The AZO samples were exposed to a varied temperature and humidity cycle, completed or not by a daily deposition of $(NH_4)_2SO_4$ or NaCl aerosols, typical pollutants in rural and marine environments, respectively. The samples exposed with and without the pollutants were compared after 1 and 2 weeks of the test. Optical transmittance and conductivity significantly degraded only for the samples exposed with the pollutants. Raman spectroscopy, X-ray diffraction and X-ray photoelectron spectroscopy evidenced localized dissolution of the AZO film and chemical modification of the Al_2O_3 encapsulation. The most severe degradation was caused by $(NH_4)_2SO_4$, which was attributed to the high stability of soluble [Zn $(NH_3)_4^{2+}$] complexes. The Al_2O_3 encapsulation improved chemical and physical stability of AZO in the presence of $(NH_4)_2SO_4$ but not in the presence of NaCl. The latter can be explained by pitting corrosion of Al_2O_3. Optical transmission curves are coherent with the AZO layer thinning in the presence of NaCl and very localized AZO dissolution (most likely grain boundary etching) in the presence of $(NH_4)_2SO_4$. The enhanced degradation of encapsulated AZO in the presence of atmospheric aerosol pollutants suggests that they cannot be neglected in the evaluation of barrier protection capacities of novel encapsulates and, more generally, in the outdoor durability assessment of novel photovoltaic materials and devices.

KEYWORDS

Al:ZnO transparent conductive oxide, Al_2O_3-encapsulation, atmospheric pollutants, flexible photovoltaics, outdoor durability

1 | INTRODUCTION

To guarantee reliability of newly developed photovoltaic (PV) modules for several decades, the relevant failure mechanisms of PV materials and their assemblies need understanding. These mechanisms can be analysed for the modules that have been in service for 25–35 years now.[1-3] Failure modes of newly developed materials can, however, only be obtained by employing some specific accelerated degradation procedures. A reliable accelerated test should favour the degradation mechanisms relevant for outdoor conditions, so its design requires to know the key factors controlling the environmentally assisted degradation of PV materials and assemblies. The latter is in particular true for the systems for which there is no 'in field' validated knowledge.

The common accelerated tests in the PV industry are expected to take into account the effects that are considered as the most harmful for PV modules, that is, sunlight illumination,[4] heat and humidity.[5] The chemistry of the outdoor environment is, however, not limited to humidity because different gaseous pollutants and aerosols can penetrate the system.[6] Some effects of complex chemical environments are considered in specific tests,[7] including immersion in liquid ammonia (IEC 62716:2013) and salt spray mist exposures (IEC 61701:2011, IEC 60068-2-52:2017). These tests are used for the qualification of PV modules expected to serve in humid atmospheres with high concentrations of dissolved ammonia (possible for farm integrated PV systems) or chlorides (coastal climate). They are, however, mainly used to assess the corrosion resistance of the metallic parts of the modules (bus-bars, cables, frames, electrical contacts, etc.), whereas no examination is made to investigate the effects of changing chemistry on non-metallic PV materials. Although water ingress in solar cells has been seriously studied in numerous scientific works (see, for instance, previous works[8–10]), the effects of chemical pollutants, such as gases and aerosols, on the stability of PV materials are rarely discussed in the scientific PV community and are not considered in the common accelerated tests. This is mainly because the aerosols penetration into fully protected encapsulated systems, and hence their interactions with the active PV materials, are expected to be minor. The ions could be, however, leached from the aerosol salts, accumulated on the surface, and infiltrate PV systems in a soluble form.

The common practice to protect PV modules from humidity is to use glass in combination with thick organic encapsulates, for example, ethylene-vinyl acetate (EVA) or polyvinyl butyral (PVB).[3] The added value of thin layer PV technology, like copper indium gallium selenide Cu (In,Ga)Se_2 (CIGS) solar cells, is that they offer a possibility to produce flexible modules,[11] for which the protection by thick glass-glass assembly is not interesting. These modules use thin polymeric front/back sheets which are lightweight and flexible. Humidity is regarded as the main durability issue for CIGS cells,[12] and water resistant thin inorganic films are studied as a complement or an alternative for poor moisture resistant polymeric materials. Thus, less than 100 nm thick Al_2O_3 films grown by atomic layer deposition (ALD) have been suggested to effectively encapsulate CIGS solar cells and modules.[13,14]

For CIGS solar cells/modules, the observed primary failure mode is degradation of the most used transparent conductive oxide (TCO), that is, the Al-doped zinc oxide Al:ZnO (AZO).[15] Flexible modules are susceptible to mechanical stress (e.g., bending and deformation), thus most likely prone to form temporary or local cracks through which chemical pollutants can penetrate and degrade the underlying active material. Some works[8–10,15–17] have considered effects of humidity and atmospheric gases such as CO_2 and O_2 on the stability of CIGS and in particular on the AZO, introducing pollutants in humid gases or in immersion conditions. The effects of the atmospheric gases have been, however, studied only for non-encapsulated systems, assuming that any encapsulation layer is enough strong to completely block the access of the gaseous and particulate constituents. The presence of atmospheric pollutants can, however, strongly affect transport properties and chemical resistance of both inorganic[18] and organic[19,20] materials used for the encapsulation. Moreover, if moisture is considered to be able to penetrate through the encapsulating layer, the dissolved atmospheric pollutants also could do it. Their effects on the encapsulated CIGS systems should be hence considered.

Another aspect, unexplored in the literature, concerns the effects induced by the accumulation of salt aerosols, deposited at atmospheric conditions. Nature and quantities of the deposited salts, as well as the corrosivity of the formed aqueous layers, strongly depend on the climate and atmospheric pollutants levels.[6,21,22] Variations in soluble salt composition and concentration can strongly influence atmospheric stability of exposed materials. As demonstrated previously by the accelerated ageing tests of painted metallic materials in automotive applications, disregarding these variations in accelerated tests can lead to materials ranking which is different from the ranking observed in outdoor exposure.[23] The effects of the atmospheric aerosol pollutants are currently not considered in the durability assessment of PV materials.

In all, effects of atmospheric chemistry on the degradation mechanisms and durability of PV systems, and in particular on non-metallic materials, are generally disregarded. To support or disclaim the necessity to introduce these species into accelerated degradation procedures, the degradation mechanisms of novel materials with and without these species should be approached. This calls for new test procedures[15] in which the physical characterization after accelerated ageing is accompanied by advanced chemical analysis.

The main objectives of this study are

1. to demonstrate, using the methodology inherited from corrosion science, that atmospheric pollutants such as aerosols of NaCl or $(NH_4)_2SO_4$, can significantly affect chemical and physical stability of functional materials and encapsulates in PV;
2. to present a new comprehensive testing procedure, taking into account the effect of atmospheric aerosol pollutants, and apply it to Al_2O_3-encapsualted AZO thin films.

Although the behaviour of the material in a full stack of layers in solar cells can be more complex than in the studied model system, its intrinsic stability is still important for the understanding of the full system.

Moreover, the proposed methodology, taking into account the effect of atmospheric aerosol pollutants, can be further extended to more complex systems including cells and modules.

1.1 | Accelerated ageing procedure design

The choice of the specific accelerated ageing procedure, climatic testing, was inspired from atmospheric corrosion methodology. This practice includes accelerated ageing in a climatic chamber combined with advanced chemical characterization at different time points. The chamber can recreate in a controlled way environmental and weather stresses that the tested material could encounter at outdoor conditions, for example, variations of temperature, humidity, differences in salt deposition and of gaseous pollutant levels. The proposed climatic test is schematically shown in Figure 1. In short, the temperature (T°C) and relative humidity (RH) were cycled (T°C: 4 h 25°C ⇒ 4 h 80°C ⇒ 4 h 25°C, RH: 2 h 20% ⇒ 2 h 90% ⇒ 4 h 20% ⇒ 4 h 90%) and salt aerosols (NaCl or $(NH_4)_2SO_4$) were deposited every 24 h during the first week of exposure. The temperature of 80°C was selected to approach the extreme overheat that is possible for PV systems.[7] The lowest temperature (25°C) was chosen to simulate manual daily salt deposition. Relative humidity variations between 20% and 90% are typical for the European climate.[6,21] The complete test duration was 7 days (1 week) and 14 days (2 weeks). Two different salts, $(NH_4)_2SO_4$ and NaCl, were sprayed onto the surfaces using an airbrush (Aztec 220) once a day during the first 5 days of the first week of exposure. No salts were further deposited during the second week of exposure. The quantities of the deposited salt were 7.5 μg cm^{-2} day^{-1} for NaCl and 15.0 μg cm^{-2} day^{-1} for $(NH_4)_2SO_4$ to mimic marine and rural atmospheric conditions, respectively.[21,24]

A similar approach with cyclic RH and T°C variations and salt deposition has previously been shown to mimic corrosion mechanism of metallic materials exposed to coastal climate.[25,26] Such tests, simulating seasonal and diurnal variations, have not previously been employed for photovoltaic applications for which mainly continuous salt spray or tests using, for example, gaseous ammonia were employed (see, for instance, Mathiak et al.[27]). Outdoor conditions with high concentrations of gaseous ammonia may only be relevant for very specific conditions, possibly close to agricultural farms. Exposure to aerosols containing ammonium sulphate $(NH_4)_2SO_4$ represents a more universal exposure scenario since the salt readily forms in the presence of ammonia and sulphur dioxide and can be diffusely dispersed over longer distances.[6]

2 | MATERIAL SYNTHESIS AND CHARACTERIZATION

Al:ZnO (AZO) films of 340 ± 17 nm thickness on soda-lime glass substrate were obtained by radio-frequency sputtering according to procedures described in Zhang et al.[14] The initial thickness variation (≤10% between samples) was related to the large area (20 × 20 cm^2) of the sputtering process. Twenty-five nanometre Al_2O_3 thin films were prepared by atomic layer deposition (ALD) as described elsewhere.[28] The film thickness was selected since a previous study by some of the authors have demonstrated that a 25 nm thick Al_2O_3 encapsulation is enough to protect AZO films against degradation during 1,000 h of damp heat test (RH 85%, T 85°C).[14]

Detailed test conditions and sampling for all non-encapsulated and Al_2O_3-encapsulated AZO materials are summarized in Table 1. Three encapsulated and three non-encapsulated samples were tested in each of three climatic conditions: cyclic RH/T°C variation without salt deposition (blank), cyclic RH/T°C variation with NaCl deposition and cyclic RH/T°C variation with $(NH_4)_2SO_4$ deposition. Three other samples of each type were stored in the desiccator without climatic ageing for reference purposes.

Surface degradation as a result of the accelerated test was monitored by visual inspection and optical imaging during the salt deposition procedure (examples of the surface appearance are given in the supporting information, Figure S5). After 1 and 2 weeks of the accelerated tests, the samples were characterized by means of X-ray diffraction (XRD), Raman and Photoluminescence (PL) spectroscopy, light optical microscopy (LOM), UV-Vis-NIR spectrophotometry and sheet resistance (R_s) measurements. XRD and Raman analysis were performed twice: (i) on the samples directly taken from the climatic chamber and dried in air, so considering the presence of soluble salts, and (ii) after the samples had been rinsed with deionized water,

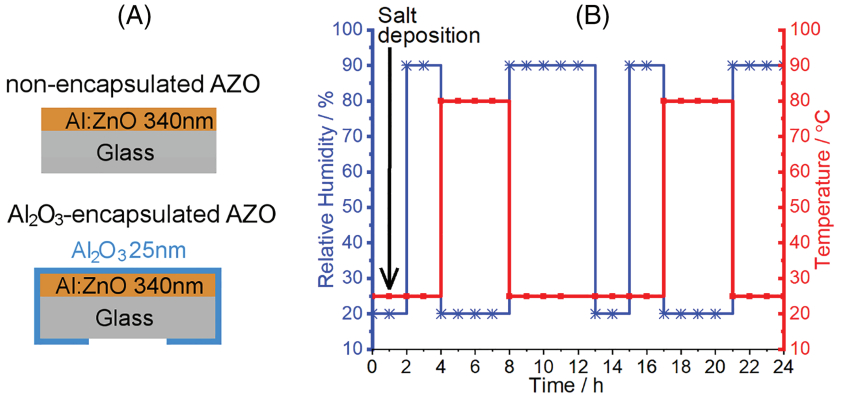

FIGURE 1 Schematics of (a) sample configurations and (b) 1-day (24 h) cycle of new climatic test. The test duration was 7 or 14 days. In both cases, salt was deposited only during the first 5 days

TABLE 1 Detailed description of the climatic test conditions for all AZO samples in this study

Sample name	Climatic test conditions	# samples for A	# samples for B
Unexposed	No exposure	3	3
Blank	T°C + RH cycling for 2 weeks	3	3
NaCl_1week	T°C + RH cycling + NaCl, 1 week	3	3
NaCl_2week	T°C + RH cycling + NaCl, 2 weeks	2	2
$(NH_4)_2SO_4$_1week	T°C + RH cycling + $(NH_4)_2SO_4$, 1 week	3	3
$(NH_4)_2SO_4$_2weeks	T°C + RH cycling + $(NH_4)_2SO_4$, 2 weeks	2	2

Note: "A" for non-encapsulated AZO and "B" for Al_2O_3-encapsulated AZO.

removing the deposited soluble salts, and dried by nitrogen flow. Analysis before and after rinsing allowed to observe modification of the AZO layer and to identify separately soluble and insoluble products. Other characterizations were made on the rinsed samples.

Bragg-Brentano XRD diffractograms were collected using Cu Kα radiation on a PANalytical Empyrean equipment in the 2θ range of 10–90° with a step size of 0.0263°. The optical transmittance was recorded on a UV-Vis-NIR spectrophotometer (Perkin Elmer Lambda 950) equipped with an integrating sphere. The sheet resistance, R_s, was measured with an in-line 4-point probe (LucasLab Probe 4 apparatus). Raman and room temperature PL spectra were recorded at room temperature using a Horiba LabRAM confocal Raman microscope with a UV laser. The UV laser ($\lambda = 325$ nm/3.8 eV) energy is close to the band gap energy of ZnO (~3.3 eV) allowing resonant conditions. In these conditions, the Raman spectra of AZO are characterized by a broad band in the range of 350–525 cm^{-1} which shape, and intensity can be correlated with the doping level and free carrier density.[29,30] The laser power (0.04 mW) was optimized in a way to obtain the signal of a sufficient intensity with a reasonable acquisition time and to avoid heating effect. The surface of the samples was examined using an advanced confocal laser scanning microscope (Olympus LEXT OLS5000) which allows 3D surface profile acquisition.

X-ray photoelectron spectroscopy was used to study changes in the chemical composition of the outermost surface (1–3 nm) of the encapsulated samples. XPS spectra were recorded using a Kratos AXIS UltraDLD X-ray photoelectron spectrometer (Kratos Analytical, Manchester, UK) using a monochromatic Al X-ray source (300 W). The analysis area was smaller than 1 mm^2 (most of the signal originated from an area of 700 × 300 μm^2). Wide and detailed spectra of Zn 2p, Al 2p, O 1 s and Si 1 s (and C 1 s for energy correction to 285.0 eV) were acquired using a pass energy of 20 eV to determine changes in oxidation states of Zn and Al and to assess Al to Zn (Al/Zn) and Al to O (Al/O) atomic ratios.

Localized depth profiles were obtained for the Al_2O_3 encapsulated AZO exposed for 2 weeks of climatic test without any salt deposits by means of Scanning Auger Nanoprobe Phi 700 with Coaxial Cylindrical Mirror Analyser (CMA) operating with a primary electron beam voltage of 10 kV. The sample was tilted 30° which resulted in the detection at 60° tilt (considering the CMA collection tilt 30°). Profiling was fulfilled with layer by layer sputtering using Ar gas at 2 kV and a current density of 1 $\mu A \cdot mm^{-2}$ during the first 30 cycles followed by 4 $\mu A \cdot mm^{-2}$ during the remaining analysis. The duration of each cycle was 10 min, each with an acquisition of 60 s. Zinc (Zn) was monitored in the window between 958 to 1,018 eV, aluminium (Al) from 1,356 to 1,416 eV and oxygen (O) from 472 to 532 eV. Silicon (Si) was used as a marker of the glass substrate and recorded in the window between 1,580 and 1,640 eV. Once the glass substrate was reached (growth of the Si signal), the measurement was rapidly stopped since charge accumulation makes the results ambiguous and can also modify the sample. The equivalent sputtered depth was calculated from the sputtering time, assuming the sputtering rate of all layers to be similar to the sputtering rate of SiO_2 at similar conditions.

3 | RESULTS

3.1 | Effect of NaCl and $(NH_4)_2SO_4$ deposits in climatic test on physical characteristics of AZO

3.1.1 | Optical transmittance and sheet resistance

The optical transmittance of non-encapsulated and Al_2O_3-encapsulated AZO films after exposure in the climatic test with and without the presence of salts is presented in Figure 2. Sheet resistance, R_s, values are indicated next to the corresponding transmittance curve for the non-encapsulated AZO films (Figure 2a). Sheet resistance is not indicated for the Al_2O_3-encapsulated AZO layer (Figure 2b) because it was not measured under insulating Al_2O_3 layer.

For the non-encapsulated AZO samples (Figure 2a), the R_s of the blank sample (2 weeks' exposure without salt) was close to that of the unexposed sample. Small differences (~10%) could be due to initial thickness variations and batch-to-batch differences. The results indicate that the exposure to the cyclic temperature and humidity variation without salt deposition does not significantly affect the optoelectrical properties of non-encapsulated AZO. After the same temperature and humidity cycle with NaCl deposition, the R_s was 1.5 (after 1 week) and 2 (after 2 weeks) times higher than that of the blank sample, and the transmittance in the near infrared region increased with time (Figure 2a), which was not observed in the absence of the salt. The transmittance of TCOs in the near infrared region is known to increase with reduced free carrier concentration.[31,32] This suggests that the deposition of NaCl during the climatic

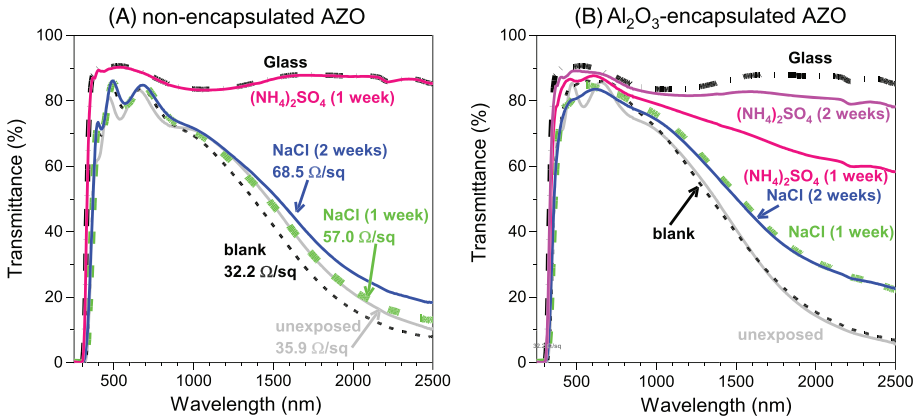

FIGURE 2 Optical transmittance of (a) non-encapsulated AZO and (b) Al_2O_3 encapsulated AZO samples. Results for unexposed, blank (2 weeks' exposure without salt), and exposed with NaCl or $(NH_4)_2SO_4$ deposits for 1 and 2 weeks are shown, as indicated

test may lead to a loss of free carriers. After only 1 week of the test with $(NH_4)_2SO_4$, the transmittance curve of the AZO sample overlapped with the curve of bare glass and R_s was no more measurable. This suggests severe degradation or even complete removal of the AZO film.

In a similar manner, optical transmittance evolved for the Al_2O_3-encapsulated AZO samples (Figure 2b). Interestingly, after 1 week of the test with NaCl, the encapsulated samples showed even more pronounced increase of transmittance in the near infrared region than non-encapsulated samples. In contrast, in the presence of $(NH_4)_2SO_4$, the transmission evolution was slower for the Al_2O_3-encapsulated samples than for non-encapsulated samples.

To sum up, although the 25 nm thick Al_2O_3 encapsulation seems to prevent physical degradation of AZO films in conditions of varying temperature and humidity, which is coherent with the previously reported results of 1,000 h damp heat test,[14] it is clearly insufficient to prevent AZO degradation in the same temperature and humidity variations in the presence of the atmospheric aerosols (NaCl and $[NH_4]_2SO_4$).

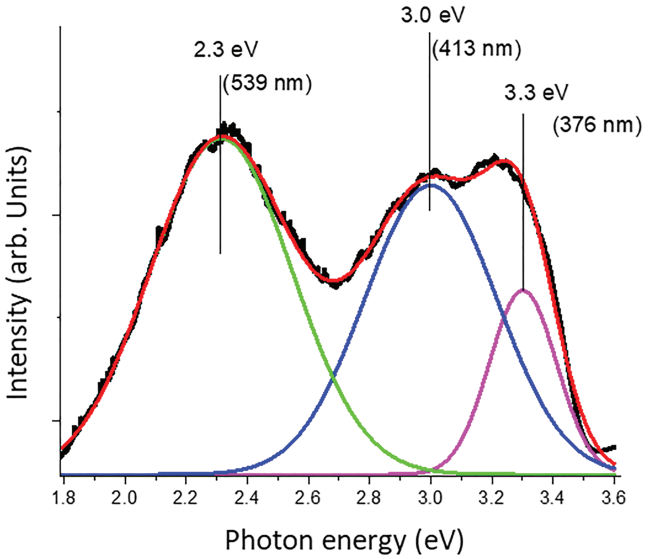

FIGURE 3 Example of room temperature photoluminescence spectrum of unexposed AZO

3.1.2 | Photoluminescence spectra

An example of a photoluminescence (PL) spectrum of an unexposed non-encapsulated AZO sample is presented in Figure 3. The spectrum contains three typical for AZO emission peaks: a near band edge emission at, or above, 3.3 eV (the full emission was cut by the edge filter), a broad band approximately at 3 eV and a deep emission band at 2.3 eV. The broad band occurring at 3 eV has previously been attributed to intrinsic defects (interstitial Al or Al_i).[33] Emission at 2.3 eV is typical for both undoped (pure) and Al-doped ZnO and is often attributed to oxygen vacancies or other oxygen-related point defects.[33–35] The emission peak contributions varied between different locations of the same sample and also among different samples (see supporting information, Figure S1a). This is the most probably related to an initial inhomogeneity in the defect distribution inside the film. The band at 3 eV was in general more pronounced for the encapsulated compared with non-encapsulated samples (see example in supporting information, Figure S1a). This could possibly be related to an increased number of active Al-dopants in the AZO films during the ALD deposition (160°C) of Al_2O_3. Investigations of samples exposed to the climatic test demonstrated similar room temperature PL spectra and similar variations between the samples (see supporting information, Figure S1b). Thus, no clear statistically valid difference was evidenced between unexposed and exposed samples (either to cyclic T°C/RH or to T°C/RH combined with the aerosol salts deposition). This suggests negligible changes in the bulk electronic state of the degraded AZO thin films.

3.2 | Effect of NaCl and $(NH_4)_2SO_4$ deposits on chemical composition after climatic test

3.2.1 | X-ray diffraction: Crystalline phases in AZO layer

The examples of XRD diffractograms of pristine (non-encapsulated) and Al_2O_3-encapsulated AZO samples after different exposures and rinsing are presented in Figure 4a,b, respectively. The spectra before

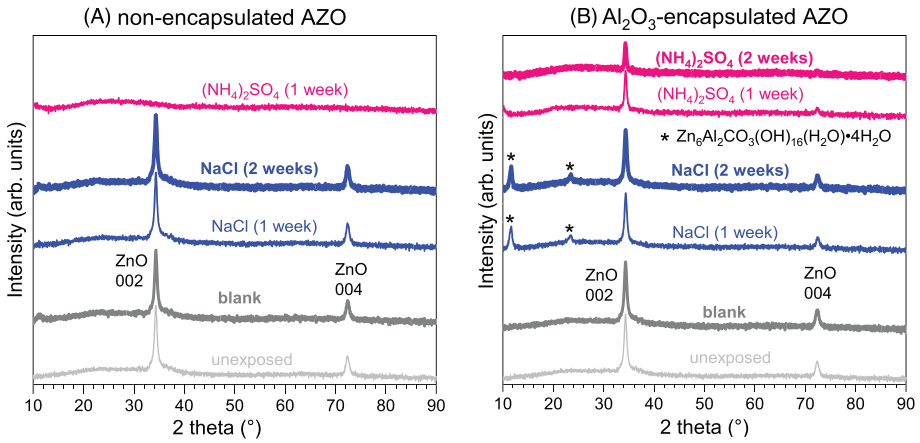

FIGURE 4 Bragg-Brentano XRD of (a) non-encapsulated AZO and (b) Al_2O_3-encapsulated AZO samples after climatic test. The test duration is indicated for the samples exposed with NaCl or $(NH_4)_2SO_4$, blank sample was exposed for 2 weeks without salt. The reference patterns are ZnO (JCPDS 00–036-1,451) and $Zn_6Al_2CO_3(OH)_{16}(H_2O)•4H_2O$ (JCPDS 00-038-0486)

rinsing, which reflects soluble salts deposits, can be seen in supporting information, Figure S2. Since the ALD grown Al_2O_3 layer is very thin and amorphous, it does not contribute to any diffraction peaks. The polycrystalline AZO films showed a preferred orientation (002) with a strong ZnO (002) diffraction peak centred at 34.34° ± 0.04° (2θ). A slight difference of the initial peak position, if compared with a standard ZnO powder ($2\theta = 34.42°$), could indicate a slight compressive stress related to doping. No shifts of the peak positions were observed for any of the samples exposed in the climatic chamber. These results imply no significant structural changes of AZO in the cyclic T°C/RH variation with or without aerosol salt deposition. Small changes in peak areas can hence indicate the material loss or crystallinity loss.

For the non-encapsulated AZO films (Figure 4a), similar XRD spectra were observed for unexposed and NaCl-exposed samples (both after 1 and 2 weeks). This suggests negligible material loss. No XRD peaks were observed for the samples exposed to $(NH_4)_2SO_4$ for 1 week, which is consistent with the previously discussed transmittance results of the same samples, showing similar transmittance curves as the glass substrate. Hence, the unprotected AZO film seems to be completely dissolved by $(NH_4)_2SO_4$ introduced in the climatic test.

For the Al_2O_3-encapsulated AZO thin films, AZO was preserved not only in the tests with NaCl, but also in the presence of $(NH_4)_2SO_4$, Figure 4b. Still, the (002) peak area decreased faster for the samples exposed to $(NH_4)_2SO_4$ than for samples exposed to NaCl (Table 2). Two additional peaks (marked with * in Figure 4) at 11.6° and 23.4° (2θ) are visible in the figure for the NaCl-exposed samples. These peaks correspond to Zn-Al-layered double hydroxide (LDH) $Zn_6Al_2CO_3(OH)_{16}·4H_2O$ (JCPDS 00-038-0486). This compound is known as atmospheric corrosion product formed on Zn-Al alloys.[25,36] It is interesting to note that the ZnO (002) peak area was reduced for the encapsulated AZO upon exposure to NaCl, while it remained unchanged for non-encapsulated AZO exposed in parallel. The presence of Al_2O_3 seems hence to enhance rather than to protect AZO from degradation in the presence of NaCl aerosols.

The crystallite size in the (002) direction (34 ± 4 nm), calculated using Scherrer equation, seemed to be unaffected by the climatic tests for both non-encapsulated and Al_2O_3-encapsulated AZO (Table 2). This indicates that the grain dissolution, if taking place, is negligible along the vertical direction (direction of the film growth).

XRD analysis of the non-rinsed non-encapsulated AZO samples exposed to NaCl showed the presence of zinc hydroxychloride (simonkolleite) $Zn_5(OH)_8Cl_2·H_2O$ (JCPDS PDF 00-007-0155). Since this compound was not detected after careful washing with deionized water (Figure 4a), it can be considered as either a soluble or poorly adherent degradation product. One could consider also that the crystalline simonkolleite is transformed into an amorphous form; however, there is no reason to think that such a transformation can be induced by a simple washing at room temperature. Another possibility is that a very thin layer of the product is not detected by XRD after washing. Similarly, a mixture of sulphate salts, including zinc hydroxysulphates and ammonium sulphates, was observed on non-washed surfaces (see supporting information, Figure S2) but not after rinsing on either the encapsulated or non-encapsulated AZO samples exposed to $(NH_4)_2SO_4$. The signature of sulphate anion was also detected by Raman spectroscopy before washing (as illustrated in supporting information by a sharp band indicated in Figure S3) but not after it. Similar reasoning as used for simonkolleite implies the formation of mainly soluble or non-adherent sulphate-containing compounds during AZO degradation in the presence of $(NH_4)_2SO_4$. S and Cl were also detected on the surface by electron dispersion spectra (EDS) microanalysis in scanning electron microscope (see supporting information, Figure S6).

3.2.2 | Confocal optical microscopy: Surface inhomogeneity

Examples of confocal optical images of the pristine and Al_2O_3-encapsulated AZO thin films after climatic tests and rinsing are presented in Figure 5. Unexposed samples are also shown for comparison, demonstrating smooth and homogeneous surface. For the non-encapsulated AZO thin films exposed to NaCl (Figure 5a) and for the Al_2O_3-encapsulated AZO thin films exposed to either NaCl or $(NH_4)_2SO_4$ (Figure 5b), the images show an optical contrast and specific regions can be distinguished, which are marked by red arrows. The measured height in these regions was approximately 340 nm lower than in the surrounding zones. This height difference correlates well with the thickness of the AZO layer, which indicates its local dissolution. Hence, it seems that the AZO could, as a consequence of salt

deposition, be locally transformed into soluble/or loosely attached compounds that easily can be washed from the surface.

3.2.3 | Raman spectroscopy: Changes in AZO layer chemistry

Confocal Raman spectroscopy analysis was conducted to confirm the hypothesis of partial localized dissolution of the AZO layer in the presence of salts. Representative Raman spectra of the different dissolved areas marked in Figure 5 are presented in Figure 6. One should remember that the images in Figure 5 and the spectra shown in Figure 6 are obtained after rinsing of the samples. The results show similar spectra for all locations of the non-encapsulated AZO sample after 1-week exposure to $(NH_4)_2SO_4$ (spectra 4a) as observed for the glass substrate. This confirms complete dissolution of the AZO film, findings which are consistent with the both the transmittance and the XRD results. Similar Raman spectra as observed for glass were also evident for the locally dissolved areas (marked with red arrows in Figure 5) on both non-encapsulated (spectrum 4a) and Al_2O_3-encapsulated (spectrum 4b) samples. These results confirm the hypothesis of localized dissolution of the AZO layer in these areas.

The Raman spectra, collected with an ultraviolet (UV 325 nm) excitation wavelength, denoted 1a, 1b, 2a, 2b and 3a, 3b in Figure 6

Sample name	$ZnO_{(002)}$ peak		
Non-encapsulated AZO	**Position (°)**	**Area (arb. Units)**	**Crystallite size (nm)**
Unexposed	34.34 ± 0.04	4,835	33
Blank	34.33	4,418	36
NaCl_1week	34.33	5,064	37
NaCl_2week	34.32	5,430	38
Al_2O_3-encapsulated AZO	Position (°)	Area (arb. units)	Crystallite size (nm)
Unexposed	34.30	3,829	32
Blank	34.32	4,307	34
NaCl_1week	34.35	2,135	32
NaCl_2weeks	34.34	2,589	34
$(NH_4)_2SO_4$_1week	34.32	912	31
$(NH_4)_2SO_4$_2weeks	34.30	341	34

TABLE 2 Characteristics of (002) peak of ZnO for the samples after climatic tests with different exposure conditions defined in Table 1

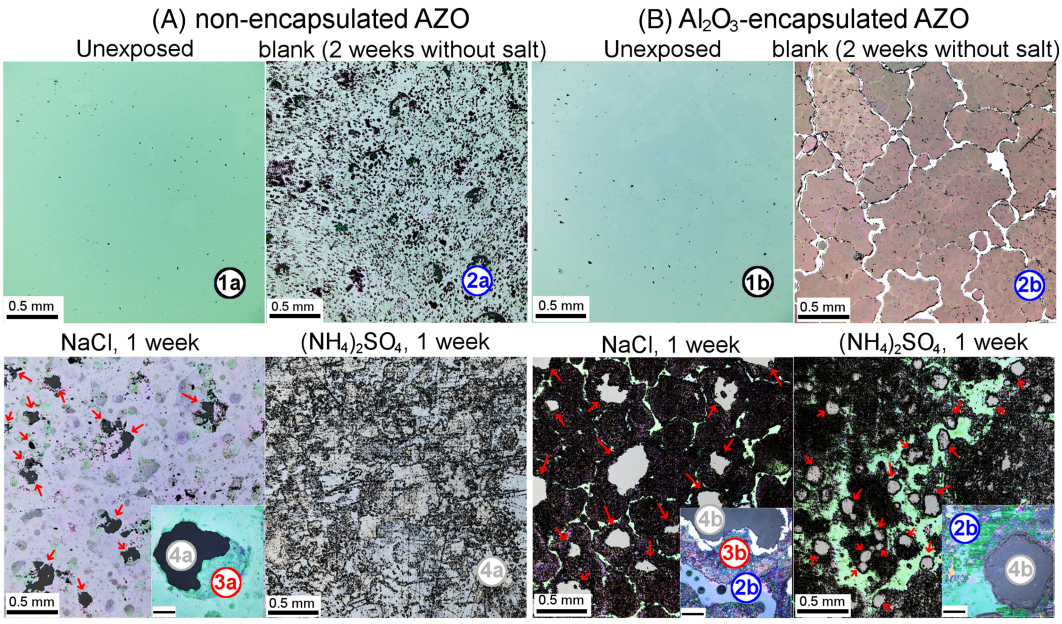

FIGURE 5 Confocal optical microscope images of (a) non-encapsulated and (b) Al_2O_3-encapsulated AZO samples. High-resolution optical images are shown in insets (scale bar 50 μm). Red arrows indicate locally dissolved areas in which the height is approximately 340 nm lower than in the surrounding areas. Exposure conditions (cycling time and salt used for the aerosol deposit) are indicated

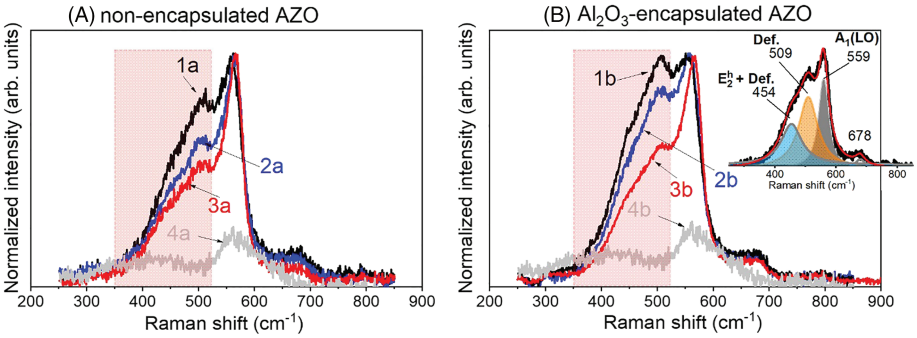

FIGURE 6 Representative Raman spectra of different zones of (a) non-encapsulated and (b) Al_2O_3-encapsulated AZO thin films exposed to different climatic test conditions. The labels reflect the zones of different types, shown in Figure 5. Spectra 1–3 are normalized by the A_1(LO) band of ZnO. Spectra 4a and 4b coincide with the Raman spectra of the glass substrate. The inset in (b) illustrates an example of the peak fitting performed by 3 Lorenz curves

are typical for the AZO thin film. The spectra show an intense peak at ~560 cm^{-1} together with a so-called 'defect band' (shaded region in Figure 6a,b) in the range of 350–525 cm^{-1}. Detailed deconvolution of the spectra is exemplified in the inset of Figure 6b. The band at approximately 559 cm^{-1} (filled in grey) has previously been attributed to the vibrational modes E_1(LO) and A_1(LO) of ZnO.[35,37] This band, in the following denoted LO, dominated all spectra. The lower frequency band contains two contributions, which both are attributed to the presence of defects in the structure of ZnO. The band at approximately 510 cm^{-1} is known as the 'anomalous' vibrational mode, appearing when ZnO is n-doped (by Al,[29,30,37] Mn[38] or Fe, Sb, Ga, Li[39]). The higher contribution of this band, observed for the encapsulated AZO samples, could be explained by an 'annealing' effect achieved at 160°C during the ALD deposition of Al_2O_3 (as previously mentioned for the room temperature PL spectra). The component centred at around 454 cm^{-1} (shaded in blue) can be attributed to the superposition of both the E_2^h mode of ZnO (doped or undoped, 437–438 cm^{-1})[37] and the 'defect' band. The relative area fraction of the broad band between 350 and 525 cm^{-1} (convoluting both peaks of 454 and 510 cm^{-1}) was empirically correlated with the resistance of the AZO layers, which showed the resistance to be reduced as the relative area of this broad band increased.[29] For the samples exposed to NaCl (spectra 3a and 3b) and $(NH_4)_2SO_4$ (spectra 2b), it is evident that the area of this band was reduced as compared to the unexposed samples (spectra 1a, 1b). A decrease of the area of the band around 500 cm^{-1} was also observed for the blank samples (2 weeks of exposure without any salt deposition). The results suggest that the degradation of the AZO thin films exposed to the climatic test (both with and without salt deposition) is inhomogeneous and can lead to a local increase of the resistance.

Furthermore, along with the reduced intensity of the broad band, the position of the major LO band (see Table 3) indicated a red shift (from 557 to 564 cm^{-1}). The full width at half maximum (FWHM) of the band seemed to be reduced only for the non-encapsulated samples. The LO band position and its FWHM have been reported in the literature to depend on the oxide stoichiometry and doping level[29,38,40] (the lower the O_2 partial pressure used during the AZO deposition, the less resistant was the layer, and the lower LO band wavelength, the larger was the FWHM[29]). A reduced FWHM and the red shift observation of the LO band could be hence regarded as an indication of a local modification of the stoichiometry of the residual oxide.

TABLE 3 *Position and full width at half maximum (FWHM) of LO mode in Raman spectra of AZO illustrated in* Figure 5

Spectrum number	Peak position (cm^{-1})	Peak FWHM (cm^{-1})
Non-encapsulated AZO (Figure 3a)		
1a	559	39 ± 1
2a	563	34 ± 1
3a	564	30 ± 1
Al_2O_3-encapsulated AZO (Figure 3b)		
1b	557	42 ± 1
2b	558	39 ± 1
3b	564	33 ± 1

3.2.4 | X-ray photoelectron spectroscopy: Chemical changes in Al_2O_3—Encapsulation

XPS was conducted in order to assess changes in chemistry of the thin and amorphous Al_2O_3 encapsulation layer which was not detectable by means of Raman spectroscopy. The results are presented in Table 4.

Since the thickness of the as-grown Al_2O_3 film (25 nm) exceeds the probing depth limit of XPS (1–3 nm), no zinc signal from the AZO layer would be obtained for the unexposed sample, and/or samples exposed to the climatic tests with and without salt deposition if the Al_2O_3 encapsulation remains undamaged. This was indeed the case for the unexposed and blank Al_2O_3-encapsulated AZO samples (Table 4). Compositional analyses showed atomic ratios of Al to O of 0.58 ± 0.04, that is, close to the theoretical value of 0.66. The discrepancy with a higher O content was predominantly assumed to be

TABLE 4 Average atomic ratios of Al, O and Zn and list of pollutants detected on the top surface of the samples exposed in climatic chamber in different conditions

Non-encapsulated AZO			
Exposure conditions	**Al/O ratio**	**Zn/Al ratio**	**Other elements**
Unexposed[1]	0.05	16.6	C
1 week cycling with NaCl[a]	0.10	11	Cl, Ca, Na, Si
1 weeks cycling with $(NH_4)_2SO_4$[a]	0.08	3.1	C, S, Ca, Na, Si
Al_2O_3-encapsulated AZO			
Exposure conditions	**Al/O ratio**	**Zn/Al ratio**	**Other elements**
Unexposed[a]	0.58 ± 0.02	0	C
Blank (cycling w/o salts)[b]	0.58 ± 0.04	0	C
2 weeks cycling with NaCl[a] area 1 area 2	0.08 0.40	3.6 0	Cl, Ca, Na, Si
2 weeks cycling with $(NH_4)_2SO_4$[a]	0.22	2.3	C, S

[a]Atomic ratios determined by XPS.
[b]Atomic ratios determined by AES.

connected to the presence of adventitious surface carbon contamination due to the presence of C bonded to O (C—O, C═O), and possibly also to surface hydroxylation. Degradation of the Al_2O_3 was evident for all samples when exposed to either NaCl or $(NH_4)_2SO_4$. The Al_2O_3-coated samples exposed to either $(NH_4)_2SO_4$ or NaCl for 2 weeks revealed a substantial reduction of the Al/O atomic ratio and the detection of Zn (Table 4). Exposure to NaCl furthermore resulted in local differences in composition with areas dominated by Al-rich oxides without any contribution from Zn as well as areas clearly enriched in Zn. The results clearly demonstrate a chemical modification (and hence degradation) of the Al_2O_3 encapsulation layer upon exposure to the atmospheric aerosols investigated in this study. The results imply partial and/or complete removal and dissolution of the Al_2O_3 encapsulation. The atomic ratio of Zn/Al ≅ 3.6 determined after 2 weeks of exposure to NaCl is close to the theoretical ratio (Zn/Al = 3) of the Zn-Al LDH compound detected by means of XRD. Corresponding ratio for the samples exposed to $(NH_4)_2SO_4$ was 2.3, though no identification could be done. It refers most probably to a very thin X-ray-amorphous compound as no XRD pattern was obtained for these samples. For both conditions, the Zn-signal could be de-convoluted into two peaks. This supports the presence of a several nanometres thin layer of a zinc-rich corrosion product different from ZnO or Zn $(OH)_2$ (deconvolution of Zn core level not shown).

3.2.5 | Auger electron spectroscopy: Profiling of Al_2O_3-encapsulated AZO exposed without salt

As shown in the previous sections, the presence of the Al_2O_3 film and the AZO layer of all studied areas of the blank samples (exposed for 2 weeks without salt) of the Al_2O_3-encapsulated AZO films was confirmed by XPS and Raman spectroscopy, respectively. There was, however, a visible optical contrast for these samples (see Figure 5b with white and grey regions). Different zones are also visible in the secondary electron images shown in Figure 7a. In order to verify if the contrast is due to the inhomogeneous thickness of the Al_2O_3 or the AZO layer, elemental depth profiles in different locations were recorded by means of Auger Electron Spectroscopy (AES). For two zones, marked as 1 and 2 in Figure 7a, the examples of elemental atomic concentrations of Al, O, Zn and Si as a function of sputtering time are presented in Figure 7b. To analyse these profiles, Si can be used as a marker of the glass substrate, Al as a marker of the Al_2O_3 encapsulation and Zn as a marker of the AZO layer (which contains 50 ± 5 atomic % of Zn, according the AES results).

Neither the external Al_2O_3 layer nor the glass should contain any Zn. Thus, in the Al_2O_3 layer no Zn and high Al signal are expected, while the Zn signal should sharply rise in the AZO. In practice, however, the interface can be rough, resulting in a slow and not sharp signal evolution. In this case, the interface Al_2O_3/AZO between the layers can be assumed when the Zn signal reaches approximately 50% of its intensity in the AZO. In the profiles shown in Figure 7b, the zones of the A_2O_3 layer are shaded. The Al_2O_3/AZO interfaces are shown by thin vertical dash lines. Similarly, the interface between the AZO layer and the glass substrate (marked by a thick vertical dash line in Figure 7b) is associated with an approximately 50% drop in the Zn signal and a sharp increase of the Si signal, reflecting the glass substrate. Assuming constant sputtering rate of AZO, the AZO layer thickness is reflected by the difference between the sputtering times necessary to reach the Al_2O_3/AZO and AZO/glass interfaces.

For all the analysed zones, the Al_2O_3 layer thickness (expressed in sputtering time) was similar; considering the erosion rate similar to SiO_2, the Al_2O_3 layer thickness was roughly estimated as equivalent to 30 ± 10 nm of SiO_2, that is, close to its initial thickness (25 nm). This implies that the humidity and temperature cycling without salts did not degrade the Al_2O_3 encapsulation. This observation is coherent with a previous study by some of the authors showing that the 25 nm thick layer of Al_2O_3 efficiently protects AZO thin films during 1,000 h of damp heat test.[14] In contrast, the sputtering time of the AZO layer

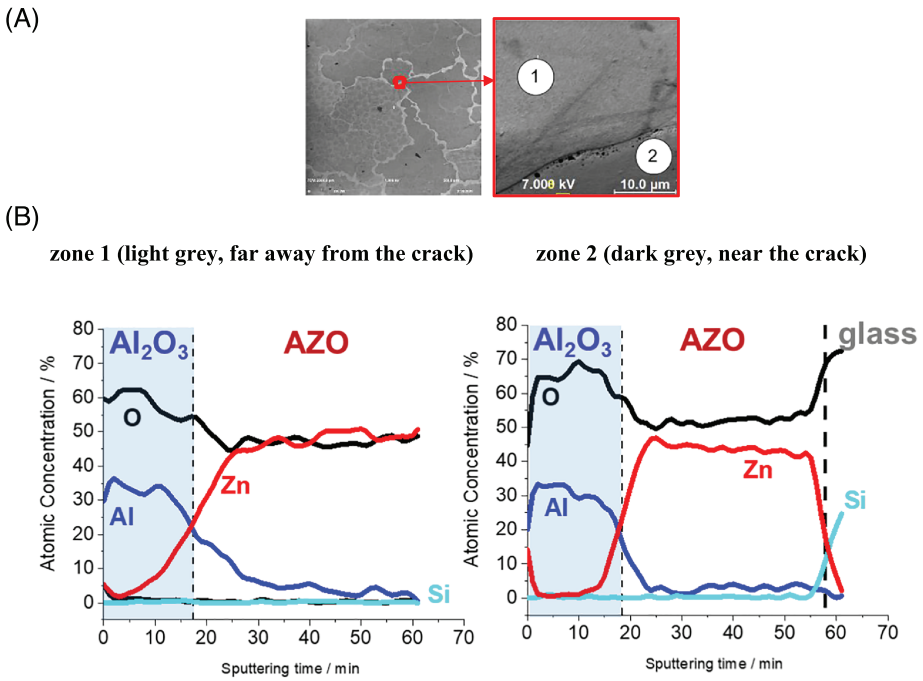

FIGURE 7 (a) Secondary electron images of blank Al_2O_3-encapsulated AZO sample after 2 weeks' exposure without salt and (b) AES depth profiles recorded in zones 1 and 2 shown in (a). Zone 1 is far away from the crack, and zone 2 is near the crack

varied for different areas by at least up to 25%. The Zn/O atomic ratios in the grey and white zones were also slightly different, which may result from the differences in local conductivity of the AZO layer and hence different sputtering rates. These results suggest hence that, despite of intact Al_2O_3 encapsulation, the colour contrast observed in the optical images of the blank sample could be due to the local AZO thickness and/or conductivity variations.

4 | DISCUSSION: EFFECT OF ATMOSPHERIC AEROSOL POLLUTANTS ON TCO STABILITY

4.1 | Chemical degradation mechanisms of AZO and Al_2O_3—Encapsulated AZO

4.1.1 | Chemical degradation of non-encapsulated AZO

Based on the XRD and optical transmittance results, it seems that the material loss was negligible for both blank samples and that the bulk structure of AZO remained unchanged. Comparative chemical and morphological analyses of the samples, exposed to the climatic tests with and without NaCl or $(NH_4)_2SO_4$, demonstrated that the deposited salts induced rapid localized degradation of AZO for both non-encapsulated and Al_2O_3-encapsulated AZO.

The AZO layer of the non-encapsulated samples was still present after 2 weeks of exposure to the cyclic temperature and humidity test but completely dissolved already after 1 week of exposure in the same temperature and humidity conditions in the presence of $(NH_4)_2SO_4$. This behaviour could be expected from the high stability of soluble complexes formed between Zn^{2+} and ammonium ions (NH_4^+) in solution, Equation 1:

$$ZnO + 2NH_4^+ = [Zn(NH_3)_2]^{2+} + H_2O. \quad (1)$$

In contrast, the effect of NaCl salt on the non-encapsulated AZO was less harmful, even though the presence of NaCl already after 1 week of the test resulted in locally observed µm- sized dissolved areas in the AZO layer. Daily deposition of NaCl resulted evidently in high local concentrations of Cl^-, creating conditions favourable for the formation of simonkolleite $Zn_5(OH)_8Cl_2\ H_2O$ (Equation 2), which is more stable than ZnO in the presence of chloride at neutral pH,[41] Equation 2a:

$$5ZnO + 2Cl^- + 5H_2O = Zn_5(OH)_8Cl_2 + 2OH^-. \quad (2a)$$

Indeed, simonkolleite was observed on the samples exposed with NaCl prior to washing. Chloride was also detected by XPS at the extreme surface of the washed samples, suggesting that probably simonkolleite was formed not only as poorly adherent precipitates but also as a several nm thick adherent layer.[42] Dissolution of ZnO via complex formation is also possible at high chloride concentrations, Equation 2b:

$$ZnO + 3Cl^- + H_2O = [ZnCl_3]^- + 2OH^-. \quad (2b)$$

The formation constant (K_f) of zinc tetra ammine complex ($K_f = 7.8 \times 10^8$) is, however, almost 9 orders of magnitude higher than for zinc tetra chloride complex ($K_f = 1.6$). This implies significant thermodynamic favouring of ZnO dissolution in the presence of ammonium salts compared to chlorides. As a result, reaction 2b initiates

from grain boundaries and requires longer time to form grooves[43] than reaction 1, which can be initiated from a non-defective surface. Additionally, the formation of low soluble corrosion products formed in the presence of chloride, for instance by reaction 2a, is expected to limit mass transfer. XPS data in Table 4 demonstrates Al enrichment at the extreme surfaces of non-encapsulated samples exposed with both salts, which could indicate a thin film of Al-rich product not detectable by XRD either because it is amorphous or too thin. The exact nature of this film is a subject of a separate study but the source of Al can be Al dopant.

Tentative chemical degradation mechanisms of non-encapsulated AZO thin films exposed to the cyclic climatic test with either deposited NaCl or $(NH_4)_2SO_4$ are schematically shown in Figure 8a,b.

4.1.2 | Chemical degradation of Al_2O_3-encapsulated AZO

The results demonstrate that thin 25 nm thick Al_2O_3 encapsulation layers protected the AZO thin films from complete dissolution during the climatic tests conducted without any salt deposition. This is coherent with the results, previously reported for similar encapsulation solutions exposed to a damp heat test.[14] At the same time, even after 1-week exposures with NaCl or $(NH_4)_2SO_4$, zones without AZO were observed on the encapsulated samples, indicating that in the presence of the pollutants this encapsulation layer was insufficient.

For the samples exposed to NaCl, the presence of the Al_2O_3 coating enhanced rather than inhibited the degradation of the AZO layer. Surface analysis evidenced the formation of $Zn_6Al_2CO_3(OH)_{16}{\cdot}4H_2O$, a corrosion product formed on Zn-Al alloys in, for example, marine environments and automotive applications.[25,36] Its formation during the climatic test with NaCl can be explained by its higher stability, compared to Al_2O_3 at slightly alkaline pH conditions, and the presence of carbon dioxide from air.[44] Considering the very low fraction of Al in the system, the detection of this Al-containing product by XRD indicates that it is well crystallized and probably textured. The observation that this LDH compound only was detected on the encapsulated samples suggests that the Al_2O_3 encapsulation participates in its formation. The instability of the Al_2O_3 encapsulation in neutral chloride solutions correlates well with the reported in Díaz et al.[18] degradation of 50-nm-thick ALD deposited Al_2O_3 films on carbon steel immersed in neutral NaCl aqueous solutions. Failure initiation of the Al_2O_3 film could be expected as a result of pitting induced by chloride ions, that is, local film dissolution.[41,42] The important point is that pitting and oxide thinning lead to partial dissolution of the oxide and formation of soluble Al species.[53,54] Possible scenario of the degradation of Al_2O_3-encapsulated AZO in the presence of Cl^- is schematically presented in Figure 8d.

Local dissolution of the Al_2O_3 film and the influence of humidity and Cl^- inside the pits are proposed to result in the transformation of AZO to simonkolleite, followed by its further dissolution induced by accumulated Cl^- (reaction 2). The literature reports that damp heat test of AZO results in formation of Zn $(OH)_2$ at the grain boundaries[45]

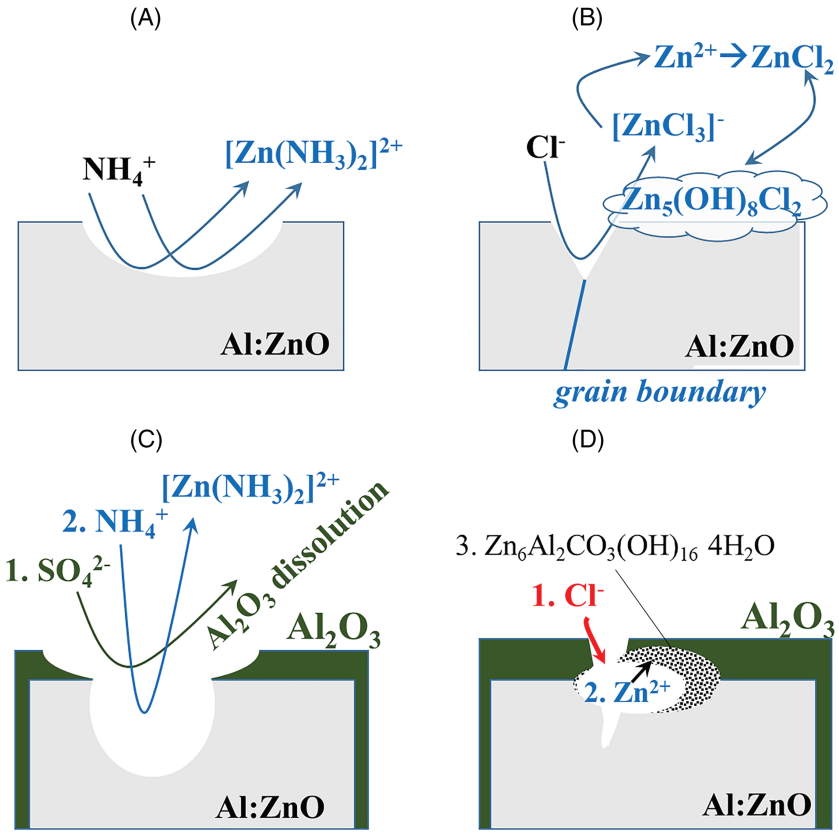

FIGURE 8 Chemical degradation of non-encapsulated and Al_2O_3-encapsulated Al-doped ZnO (Al:ZnO) layers on glass exposed in a climatic test to aerosols of NaCl or $(NH_4)_2SO_4$. (a) Dissolution of non-encapsulated AZO induced by deposited $(NH_4)_2SO_4$ via soluble Zn complexes with NH_3. (b) Local dissolution of non-encapsulated AZO induced by deposited NaCl via soluble Zn complexes with Cl^-. (c) Step 1 shows slow pit initiation with rapid pit growth of Al_2O_3 in the presence of sulphate, followed by step 2 where AZO dissolution by ammonium in areas of dissolved Al_2O_3. (d) Step 1 shows quick pit initiation in Al_2O_3 by chloride, followed by step 2 where AZO dissolution in the confined zone and step 3 where Al_2O_3 is transformed into $Zn_6Al_2CO_3(OH)_{16}{\cdot}4H_2O$ (LDH)

implying a possibility of local pH increase. Conditions with ion accumulation and local pH modification are enhanced in the confined zone beneath the Al_2O_3 film. These conditions can result in accelerated delamination and dissolution of the AZO and the Al_2O_3 encapsulation (for instance via Equation 3) followed by the formation of mixed Zn-Al hydroxides, which could be transformed into layered double hydroxide (indicated as LDH in Figure 8) by incorporating atmospheric CO_2.

$$ZnO + OH^- + H_2O = \left[Zn(OH)_3\right]^- \left(\text{and } \left[Zn(OH)_4\right]^{2-} \text{etc.}\right), \quad (3a)$$

$$Al_2O_3 + 2OH^- + 7H_2O = 2\left[Al(OH)_4\,2H_2O\right]^-. \quad (3b)$$

When the Al_2O_3-encapsulated AZO thin films were subject to $(NH_4)_2SO_4$ salt exposure, also, the Al_2O_3 encapsulation underwent dissolution. Indeed, high amounts of Zn observed in the outermost surface by means of XPS imply either complete dissolution, thinning of the layer thickness (less than 10 nm compared with the initial 25 nm) or chemical modification. In any case, the surface fraction of Al was lower, suggesting its partial dissolution.

Tentative chemical degradation mechanism of Al_2O_3-encapsulated AZO thin films in the climatic test with $(NH_4)_2SO_4$ salt exposure is schematically presented in Figure 8c. Once the ammonium ions reach the AZO layer the latter locally dissolved via reaction 1, as confirmed with Raman spectroscopy, XPS and optical microscopy. The fact that no crystalline LDH compounds were observed in the tests with $(NH_4)_2SO_4$ can be explained by different factors: (i) Sulphate ions are known to delay the initiation of pitting of aluminium oxides (but accelerate the development of already existing pits),[46,47] which could reduce the dissolution rate of Al_2O_3; (ii) amorphous compounds are formed (as indicated by XPS findings) and iii) the formation of LDH in the presence of sulphates requires much higher pH than in the presence of chlorides, as previously demonstrated by titrations.[48] The exact nature of the formed degradation products and the mechanisms of the interaction between the Al_2O_3-layer and $(NH_4)_2SO_4$ are on-going and topics for a forthcoming paper.

In all the studied conditions the diffraction domain of the (002) planes of ZnO remained constant, assuming similar crystallite height. This indicates that the dissolution of the layer most likely propagates in the direction parallel to the sample surface, probably along the grain boundaries. The latter seems logical since adsorption of reactive anions is expected to be faster at grain boundaries and the electrochemical dissolution of AZO is reported to start at grain boundaries.[43]

4.2 | Degradation of physical properties of Al_2O_3-encapsulated and non-encapsulated AZO

An effective transparent conductive oxide in thin film photovoltaics should have high transparency and low resistivity. The optoelectronic properties of both pristine and Al_2O_3-encapsulated AZO rapidly degraded in the climatic tests with salts deposits, with more severe degradation observed upon exposure to $(NH_4)_2SO_4$. The transmittance curve of the non-encapsulated samples exposed to $(NH_4)_2SO_4$ for 1 week coincided with the curve of the glass substrate, indicating complete dissolution of the AZO film. The transmittance of the non-encapsulated AZO exposed to NaCl was slightly affected in the infrared region. When the Al_2O_3-encapsulated AZO samples were compared after the climatic tests, the transmittance seemed to evolve differently between the samples tested with $(NH_4)_2SO_4$ and tested with NaCl. As previously discussed, the changes in the transmittance are due to the AZO layer dissolution, so different evolution of transmittance curve could probably indicate different degradation modes. If the AZO dissolution creates localized holes in the film while the thickness of the residual layer does not evolve significantly, the total transmittance T(X) of the film can be approximated as a linear combination of the glass transmittance, T (glass), representing the dissolved areas, and the initial transmission measured for the unexposed sample, T (unexposed), respectively, with α being the surface fraction of the holes ($0 \le \alpha \le 1$):

$$T(X) = \alpha \times T(\text{glass}) + (1-\alpha) \times T(\text{unexposed}). \quad (4)$$

If the AZO dissolution results in the film thinning, according to the Beer-Lambert law, a fairly linear relationship is expected between the ln[T(X)] against ln[T (unexposed)] in the absorption edge (i.e., 300–380 nm), with β being the fraction of the removed layer thickness:

$$\ln[T(X)] = \text{constant} + \beta \times \ln[T(\text{unexposed})]. \quad (5)$$

For the Al_2O_3-encapsulated AZO samples exposed to $(NH_4)_2SO_4$, the first model (Equation 4) applies well with $\alpha = 0.66$ after 1 week and $\alpha = 0.91$ after 2 weeks of the climatic test (see Figure S4a). This suggests localized dissolution of AZO and gradual increase of the fraction of these locally dissolved areas with testing time. Equation 4, however, does not fit well the transmittance curves of the Al_2O_3-encapsulated AZO tested with NaCl. In this case, the second model (Equation 5) fits better and the thickness fraction lost after 1 and 2 weeks of the exposure is very similar ($\beta = 0.70$ and $\beta = 0.68$, respectively; see Figure S4b). Since the slopes are less than one, the results suggest that the loss of the AZO layer by the film thinning.

Interestingly, the above-discussed dissolution modes are coherent with the modes reported for the anodic dissolution of AZO in the electrolytes containing chloride or sulphate anions.[49] In the conditions of Becker et al.,[49] the anodic dissolution in the presence of sulphate anions resulted in pitting corrosion with strong preferential attack at the grain boundaries which led to a rapid resistivity increase. In contrast, for the exposures in chloride containing electrolytes, the formation of the cavern-like structures in the upper part of the layer resulted in the layer thickness decrease but in a substantially slower resistivity increase with dissolution.

The degradation of the electrical properties of the AZO film is also of primary significance for solar devices. For example, the increase in sheet resistance of AZO after damp heat test is considered as one of the main mechanisms responsible for the degradation of CIGS solar cells.[50–52] In our work, R_s of the non-encapsulated AZO

thin films indeed increased after the tests with NaCl. A small increase of transmittance in the near-infrared region seems to indicate a reduction of the free carrier concentration in these samples, which could explain the increase of R_s. The carrier concentration calculated from the plasmonic frequency was, however, in the order of 10^{19} cm^{-3} for all the samples. As suggested in the literature, an increased R_s is hence more likely a consequence of the reduced charge carrier mobility in AZO.[51] Nevertheless, local variations in carrier concentrations in AZO films most likely occurred after the climatic tests for both non-encapsulated and Al_2O_3-encapsulated AZO samples. This can be concluded from the local evolution of the resonant Raman spectra (Section 3.2.3) and the room temperature PL spectra (Section 3.1.2), in which the defects are reflected by the broad band at 350–525 cm^{-1} and the lower-energy components at 2.3 and 3 eV, respectively. Both strongly varied between different zones of the same sample after the tests. In some zones, they were significantly lower than in the unexposed samples. Localized physical degradation most likely occurred hence as a result of inhomogeneous changes in defects/dopants density, which could deteriorate the local resistance of AZO.

To sum up, 2 weeks of the test combining cyclic T°C and RH variation with daily NaCl and $(NH_4)_2SO_4$ deposition were enough to deteriorate the optoelectronic properties of Al_2O_3-encapsulated AZO thin films stable in 1,000 h damp heat test. This suggests that the outdoor reliability of TCO can be strongly compromised not only by high temperature and high humidity but also by their variations and the presence of corrosive aerosols (NaCl or $(NH_4)_2SO_4$). These aspects will eventually jeopardize the functionality and long-term stability of PV devices.

Broader interpretation of the fact that the 25 nm thick Al_2O_3 can be insufficient for the AZO protection in polluted atmospheres denies its generalization for flexible solar cells at least in strongly polluted atmospheres. Different alternative solutions can be suggested, as for example, a thicker Al_2O_3 encapsulation layer or a combination of Al_2O_3 with other materials such as TiO_2, ZrO_2 or SnO_2 in a multilayered stack, as has been proposed in organic light emitting diode (OLED) applications. Whatever is the alternative, the results of the present work suggest that the standard 1,000 h damp heat solicitation is insufficient to evaluate the atmospheric stability of the new systems and the effect of atmospheric aerosol pollutants should not be neglected.

5 | CONCLUSIONS

Strong effect of NaCl and $(NH_4)_2SO_4$, typical aerosol pollutants in marine and rural atmospheres, respectively, on the degradation mode and degradation rate of pristine AZO and Al_2O_3-encapsulated AZO was demonstrated thanks to a new accelerated ageing procedure combined with advanced characterization of aged samples. The new test considers not only humidity and temperature variations but also the chemical modifications induced by the aerosol salt deposition in atmospheric conditions.

Application of the new ageing procedure demonstrated that both optical transmittance and resistance of the pristine AZO significantly degraded in 1 or 2 weeks of the new test. Chemical analysis demonstrated that contamination by NaCl resulted in a localized dissolution of the non-encapsulated AZO layer, visible after 1 and 2 weeks of the test, while $(NH_4)_2SO_4$ completely dissolved the non-encapsulated AZO in 1 week of the test. For comparison, the physical characteristics of the reference non-encapsulated samples, exposed to the same cyclic temperature and humidity variations without any salts deposition, did not significantly degrade. Rapid dissolution in the presence of pollutants was attributed to the formation of soluble chloride and ammonia complexes. The very strong difference in the dissolution rates in the presence of $(NH_4)_2SO_4$ and NaCl could be explained by more than 8 orders of magnitude difference in the formation constants of these complexes and probably by an inhibiting effect of the surface film.

Twenty-five nanometres ALD-Al_2O_3 encapsulated AZO window layers, stable in a standard 1,000 h damp heat test, were strongly degraded after 1 or 2 weeks of the new test in the presence of NaCl or $(NH_4)_2SO_4$. Moreover, the presence of the Al_2O_3 encapsulation enhanced the degradation of AZO in the presence of NaCl. The latter was attributed to the pitting corrosion of the encapsulation, resulting in a very localized attack in confined zone. Optical transmittance evolution was coherent with two distinct dissolution schemes of AZO degradation in confined zones under the encapsulation layer: (i) layer thinning morphologically close to cavernous corrosion in the presence of NaCl and (ii) local dissolution morphologically close to pitting (most likely grain boundary etching) in the presence of $(NH_4)_2SO_4$.

In this work, the effect of the atmospheric pollutants on the degradation mechanisms and degradation rates of non-metallic materials and components of PV modules in flexible solar cells was demonstrated on the example of transparent conductive oxide and new ALD deposited 25 nm thick Al_2O_3 encapsulation. This example illustrates the interest of atmospheric corrosion expertise and related test methodologies to assess the durability of transparent conductive oxides and new encapsulation solutions aimed for atmospheric exposure. Larger interpretation of the results suggests that not only humidity and temperature variation but also the atmospheric chemistry needs considering in durability assessments of PV materials and devices.

ACKNOWLEDGEMENTS

This work was partly supported by the European project solar-era.net 'Advanced global encapsulation solutions for long term stability in industrial flexible Cu (In,Ga)Se_2 photovoltaic technologies' (DURACIS) and ADEME (convention number 1705C0009). This work was partly carried out in the framework of a project of IPVF, which has been supported by the French Government in the frame of the programme of investment for the future (Programme d'Investissement d'Avenir ANR-IEED-002-01). We would like to thank Damien Coutancier (CNRS) and Samuel Rives (EDF) for help on the sputtering deposition of Al:ZnO thin films. We are also grateful to Mikael Sundin (RISE, Sweden) for help with the XPS-analysis and Mélanie Vaudescal (Placamat, France) for help with the Auger electron spectroscopy measurement.

FUNDING INFORMATION

This research did not receive any specific grant from funding agencies in the public, commercial, or not-for-profit sectors.

DATA AVAILABILITY STATEMENT

Data will be available on request

ORCID

Shan-Ting Zhang https://orcid.org/0000-0002-9691-5867
Alina Maltseva https://orcid.org/0000-0002-3532-0480
Jean-François Guillemoles https://orcid.org/0000-0003-0114-8624
Nathanaelle Schneider https://orcid.org/0000-0001-7749-2400
Inger Odnevall https://orcid.org/0000-0003-2206-0082
Polina Volovitch https://orcid.org/0000-0001-5729-9830

REFERENCES

1. Jordan DC, Kurtz SR. Photovoltaic degradation rates—an analytical review. *Prog Photovolt Res Appl*. 2013;21(1):12-29. doi: 10.1002/pip.1182
2. Virtuani A, Caccivio M, Annigoni E, et al. 35 years of photovoltaics: analysis of the TISO-10-kW solar plant, lessons learnt in safety and performance—part 1. *Prog. Photovolt. Res. Appl.* 2019;27(4):328-339. doi:10.1002/pip.3104
3. Annigoni E, Virtuani A, Caccivio M, Friesen G, Chianese D, Ballif C. 35 years of photovoltaics: analysis of the TISO-10-kW solar plant, lessons learnt in safety and performance—part 2. *Prog Photovolt Res Appl*. 2019;27(9):760-778. doi:10.1002/pip.3146
4. Kurtz S, Wohlgemuth J, Kempe M, Bosco N, Hacke P, Jordan D, Miller DC & Silverman TJ Photovoltaic module qualification plus testing, 2013. https://www.nrel.gov/docs/fy14osti/60950.pdf
5. International Electrotechnical Commission. IEC 61215-2:2016, Int Electrotech Comm IEC 61215–22016. (2016).
6. Leygraf C, Odnevall Wallinder I, Tidblad J, Graedel TE. *Atmospheric Corrosion*. Seconded. Hoboken, New Jersey: Wiley; 2016.
7. Dunlop ED, Gracia Amillo A, Salis E, Sample T, Taylor N, European Commission, Joint Research Centre, Standards for the assessment of the environmental performance of photovoltaic modules, power conversion equipment and photovoltaic systems, 2018. http://publications.europa.eu/publication/manifestation_identifier/PUB_KJNA29247ENN (accessed May 21, 2020).
8. Pern J & Noufi R Stability of CIGS solar cells and component materials evaluated by a step-stress accelerated degradation test method, in Proc. SPIE 8472, Reliability of Photovoltaic Cells, Modules, Components, and Systems V, 84720J (16 October 2012). 2012; 10.1117/12.930541.
9. Feist R, Rozeveld S, Kern B, D'Archangel J, Yeung S and Bernius M, Further investigation of the lifetime-limiting failure mechanisms of CIGSS-based minimodules under environmental stress, 2009, in 34th IEEE Photovoltaic Specialists Conference (PVSC), 2009, pp. 002359–002363, doi: 10.1109/PVSC.2009.5411323F.
10. Coyle DJ. Life prediction for CIGS solar modules part 1: modeling moisture ingress and degradation. *Progress in Photovoltaics: Research and Applications*. 2013;21:(2):156. –172. https://doi.org/10.1002/pip.1172
11. Guillemoles J-F, Rau U, Kronik L, Schock H-W, Cahen D. Cu (In,Ga) Se_2 solar cells: device stability based on chemical flexibility. *Adv Mater*. 1999;11:957-961. 10.1002/(SICI)1521-4095(199908)11:11<957::AID-ADMA957>3.0.CO;2-1
12. Guillemoles JF. The puzzle of Cu(In,Ga)Se2 (CIGS) solar cells stability. *Thin Solid Films*. 2002;403-404:405. –409. https://doi.org/10.1016/s0040-6090(01)01519-x
13. Carcia PF, McLean RS, Hegedus S. Encapsulation of Cu(InGa)Se2 solar cell with Al2O3 thin-film moisture barrier grown by atomic layer deposition. *Sol Energy Mater and Sol Cells*. 2010;94:(12):2375. –2378. https://doi.org/10.1016/j.solmat.2010.08.021
14. Zhang S-T, Guc M, Salomon O. Effective module level encapsulation of CIGS solar cells with Al2O3 thin film grown by atomic layer deposition. *Sol Energy Mater Sol Cells*. 2021;222:110914. https://doi.org/10.1016/j.solmat.2020.110914
15. Theelen M, Daume F. Stability of Cu(In,Ga)Se2 solar cells: A literature review. *Sol Energy*. 2016;133:586. –627. https://doi.org/10.1016/j.solener.2016.04.010
16. Theelen M, Foster C, Steijvers H, Barreau N, Vroon Z, Zeman M. The impact of atmospheric species on the degradation of CIGS solar cells. *Sol Energy Mater Sol Cells*. 2015;141:49. –56. https://doi.org/10.1016/j.solmat.2015.05.019
17. Hüpkes J. Influence of atmosphere and material properties on damp heat stability of ZnO:Al. *Phys Status Solidi a*. 2016;213:(7):1796. –1800. https://doi.org/10.1002/pssa.201532966
18. Díaz B, Härkönen E, Maurice V. Failure mechanism of thin Al2O3 coatings grown by atomic layer deposition for corrosion protection of carbon steel. *Electrochim Acta*. 2011;56:(26):9609. –9618. https://doi.org/10.1016/j.electacta.2011.07.104
19. Marais S, Hirata Y, Langevin D, Chappey C, Nguyen TQ, Metayer M. Permeation and sorption of water and gases through EVA copolymers films. *Mater Res Innov*. 2002;6(2):79-88. doi:10.1007/s10019-002-0183-5
20. Shkirskiy V, Uebel M, Maltseva A, Lefèvre G, Volovitch P, Rohwerder M. Cathodic driven coating delamination suppressed by inhibition of cation migration along Zn|polymer interface in atmospheric CO_2. *Npj Mater Degrad*. 2019;3(1):1-10. doi:10.1038/s41529-018-0064-z
21. Knotkova D, Kreislova K, Atmospheric corrosion and conservation of copper and bronze, in: Moncmanová A. (Ed.), *WIT Transactions on State of the Art in Science and Engineering*, 1st ed., WIT Press, 2007: pp. 107–142. 10.2495/978-1-84564-032-3/04.
22. Salgueiro Azevedo M, Allély C, Ogle K, Volovitch P. Corrosion mechanisms of Zn (Mg, Al) coated steel in accelerated tests and natural exposure: 1. The role of electrolyte composition in the nature of corrosion products and relative corrosion rate. *Corros Sci*. 2015;90:472-481. doi:10.1016/j.corsci.2014.05.014
23. LeBozec N, Blandin N, Thierry D. Accelerated corrosion tests in the automotive industry: a comparison of the performance towards cosmetic corrosion. *Mater Corros*. 2008;59(11):889-894. doi:10.1002/maco.200804168
24. Chen ZY, Zakipour S, Persson D, Leygraf C. Effect of sodium chloride particles on the atmospheric corrosion of pure copper. *Corrosion*. 2004;60:(5):479. –491. https://doi.org/10.5006/1.3299244
25. Zhang X, Leygraf C, Odnevall Wallinder I. Atmospheric corrosion of Galfan coatings on steel in chloride-rich environments. *Corros Sci*. 2013;73:62. –71. https://doi.org/10.1016/j.corsci.2013.03.025
26. Chang T, Herting G, Jin Y, Leygraf C, Wallinder IO. The golden alloy Cu5Zn5Al1Sn: Patina evolution in chloride-containing atmospheres. *Corros Sci*. 2018;133:190-203. doi:10.1016/j.corsci.2018.01.027
27. Mathiak G, Althaus J, Menzler S, Lichtschläger L, Herrmann W, PV module corrosion from ammonia and salt mist—experimental study with full-size modules, 27th Eur. Photovolt. Sol. Energy Conf. Exhib. 3536–3540. (2012). 10.4229/27THEUPVSEC2012-4BV.3.44.
28. Le Tulzo H, Schneider N, Lincot D, Patriarche G, Donsanti F. Impact of the sequence of precursor introduction on the growth and properties of atomic layer deposited Al-doped ZnO films. *J Vac Sci Technol A*. 2018;36:(4):041502. https://doi.org/10.1116/1.5030990
29. Insignares-Cuello C, Fontané X, Sánchez-González Y, et al. Non-destructive assessment of ZnO:Al window layers in advanced Cu (In,Ga)Se_2 photovoltaic technologies. *Phys Status Solidi a*. 2015;212:56-60. doi:10.1002/pssa.201431222

30. Guc M, Tsin F, Rousset J, Romanyuk YE, Izquierdo-Roca V, Pérez-Rodríguez A. Nondestructive Raman scattering assessment of solution-processed ZnO-doped layers for photovoltaic applications. *J Phys Chem C*. 2017;121(6):3212-3218. doi:10.1021/acs.jpcc.6b11525
31. Hamberg I, Granqvist CG. Evaporated Sn-doped In_2O_3 films: basic optical properties and applications to energy-efficient windows. *J Appl Phys*. 1986;60(11):R123-R160. doi:10.1063/1.337534
32. Zhang S-T, Roussel H, Chaix-Pluchery O, et al. Polymorphism of the blocking TiO_2 layer deposited on F:SnO_2 and its influence on the interfacial energetic alignment. *J Phys Chem C*. 2017;121(32):17305-17313. doi:10.1021/acs.jpcc.7b04893
33. Thandavan TMK, Gani SMA, San Wong C, Md. Nor R. Enhanced photoluminescence and raman properties of Al-Doped ZnO nanostructures prepared using thermal chemical vapor deposition of methanol assisted with heated brass. *PLOS One*. 2015;10:(3):e0121756. https://doi.org/10.1371/journal.pone.0121756
34. Willander M, Nur O, Bano N, Sultana K. Zinc oxide nanorod-based heterostructures on solid and soft substrates for white-light-emitting diode applications. *New J Phys*. 2009;11:(12):125020. https://doi.org/10.1088/1367-2630/11/12/125020
35. Iqbal D, Sarfraz A, Erbe A. Gradient in defect density of ZnO nanorods grown by cathodic delamination, a corrosion process, leads to end-specific luminescence. *Nanoscale Horiz*. 2018;3(1):58-65. doi:10.1039/C7NH00111H
36. Zhang X, Odnevall Wallinder I, Leygraf C. Atmospheric corrosion of Zn-Al coatings in a simulated automotive environment. *Surf Eng*. 2018;34(9):641-648. doi:10.1080/02670844.2017.1305658
37. Russo V, Ghidelli M, Gondoni P, Casari CS, Li Bassi A. Multi-wavelength Raman scattering of nanostructured Al-doped zinc oxide. *J Appl Phys*. 2014;115:(7):073508. https://doi.org/10.1063/1.4866322
38. Wang JB, Huang GJ, Zhong XL, Sun LZ, Zhou YC, Liu EH. Raman scattering and high temperature ferromagnetism of Mn-doped ZnO nanoparticles. *Appl Phys Lett*. 2006;88:(25):252502. https://doi.org/10.1063/1.2208564
39. Bundesmann C, Ashkenov N, Schubert M, et al. Raman scattering in ZnO thin films doped with Fe, Sb, Al, Ga, and Li. *Appl Phys Lett*. 2003;83(10):1974-1976. doi:10.1063/1.1609251
40. Ding K, Hu QC, Lin WW, Huang JK, Huang F. Longitudinal optical phonon-plasmon coupled modes of degenerate Al-doped ZnO films. *Appl Phys Lett*. 2012;101:(3):031908. https://doi.org/10.1063/1.4737647
41. McMahon M. E., Santucci R. J., Scully J. R.. Advanced chemical stability diagrams to predict the formation of complex zinc compounds in a chloride environment. *RSC Adv*. 2019;9:(35):19905. –19916. https://doi.org/10.1039/c9ra00228f
42. Volovitch P, Allely C, Ogle K. Understanding corrosion via corrosion product characterization: I. Case study of the role of Mg alloying in Zn–Mg coating on steel. *Corros Sci*. 2009;51(6):1251-1262. doi:10.1016/j.corsci.2009.03.005
43. Pust SE, Becker J-P, Worbs J, Klemm SO, Mayrhofer KJJ, Hüpkes J. Electrochemical etching of zinc oxide for silicon thin film solar cell applications. *J Electrochem Soc*. 2011;158:(7):D413–D419. https://doi.org/10.1149/1.3583636
44. Salgueiro Azevedo M, Allély C, Ogle K, Volovitch P. Corrosion mechanisms of Zn (Mg,Al) coated steel: the effect of HCO_3^- and NH_4^+ ions on the intrinsic reactivity of the coating. *Electrochim Acta*. 2015;153:159-169. doi:10.1016/j.electacta.2014.09.140
45. Lee D-W, Kwon O-Y, Song J-K, et al. Effects of ZnO:Al films on CIGS PV modules degraded under accelerated damp heat. *Sol. Energy Mater. Sol. Cells*. 2012;105:15-20. doi:10.1016/j.solmat.2012.05.002
46. Szklarska-Smialowska Z. Pitting corrosion of aluminium. *Corros Sci*. 1999;41(9):1743-1767. doi:10.1016/S0010-938X(99)00012-8
47. Lee W-J, Pyun S-I. Effects of sulphate ion additives on the pitting corrosion of pure aluminium in 0.01 M NaCl solution. *Electrochim Acta*. 2000;45(12):1901-1910. doi:10.1016/S0013-4686(99)00418-1
48. Salgueiro Azevedo M, Allély C, Ogle K, Volovitch P, Corrosion mechanisms of Zn (Mg,Al) coated steel: 2. The effect of Mg and Al alloying on the formation and properties of corrosion products in different electrolytes, *Corros Sci* 90 (2015) 482–490. 10.1016/j.corsci.2014.07.042.
49. Becker J-P, Pust SE, Hüpkes J. Effects of the electrolyte species on the electrochemical dissolution of polycrystalline ZnO:Al thin films. *Electrochim Acta*. 2013;112:976-982. doi:10.1016/j.electacta.2013.04.167
50. Westin P-O, Neretnieks P, Edoff M, Damp heat degradation of CIGS-based PV modules, in: 21st Eur. Photovolt. Sol. Energy Conf., Dresden, Germany, 2006: pp. 2470–2473.
51. Theelen M, Boumans T, Stegeman F, et al. Physical and chemical degradation behaviour of sputtered aluminium doped zinc oxide layers for Cu (In,Ga)Se_2 solar cells. *Thin Solid Films*. 2014;550:530-540. doi:10.1016/j.tsf.2013.10.149
52. Theelen M, de Graaf F, Daume F, Barreau N, Vroon Z, Zeman M, Damp heat related degradation mechanisms within CIGS solar cells, in: 2016 IEEE 43rd Photovolt. Spec. Conf. PVSC, IEEE, Portland, OR, USA, 2016: pp. 2292–2297. 10.1109/PVSC.2016.7750045.
53. Natishan PM, O'Grady WE. Chloride ion interactions with oxide-covered aluminum leading to pitting corrosion: a review. *J Electrochem Soc*. 2014;161(9):C421-C432. doi:10.1149/2.1011409jes
54. McCafferty E. Sequence of steps in the pitting of aluminium by chloride ions. *Corros Sci*. 2003;45(7):1421-1438. doi:10.1016/S0010-938X(02)00231-7

SUPPORTING INFORMATION

Additional supporting information may be found in the online version of the article at the publisher's website.

How to cite this article: Zhang S-T, Maltseva A, Herting G, et al. Importance of atmospheric aerosol pollutants on the degradation of Al_2O_3 encapsulated Al-doped zinc oxide window layers in solar cells. *Prog Photovolt Res Appl*. 2022;30(5):552-566. doi:10.1002/pip.3527